PROCEEDINGS OF SCIENCE

Hidden exact symmetry in graphene

Tetsuya Onogi[*†]
Osaka University
E-mail: onogi@phys.sci.osaka-u.ac.jp

The emergence of massless Dirac fermion in graphene has attracted attention in recent years due to the remarkable features. The tight-binding honeycomb lattice hamiltonian to explain this feature has a close analogy with "the staggered fermion" which is widely used in lattice gauge theory. Employing the position space formalism developed in lattice gauge theory, we reformulate the tight-binding honeycomb model. We show that there exists a hidden exact symmetry at finite lattice spacing, which protects the masslessness of the Dirac fermion.

The 32nd International Symposium on Lattice Field Theory
23-28 June, 2014
Columbia University New York, NY

[*]Speaker.
[†]This talk is based on a work in collaboration with Masak Hirotsu, Eigo Shintani and Aya Kagimura.

© Copyright owned by the author(s) under the terms of the Creative Commons Attribution-NonCommercial-ShareAlike Licence.

PoS(LATTICE2014)019

1. Introduction

Graphene is a two dimensional sheet of Carbon atom havinv four valence electrons in sp^2 orbit, three of which are used for σ bond for neighboring Carbon atoms to form the honeycomb lattice structure and one of which can hop freely on the graphene sheet[1, 2, 3, 4] . One of the striking features of Graphene is the emergence of massless Dirac fermion at low energy with fermi velocity around $c/300$ [2, 5]. In condensed matter language, this correspond to the existence of special momenta K called 'Dirac points' and low energy excitation around the Dirac points with linear dispersion relation gapless mode with linear dispersion relation $E \approx \pm|k-K|$, where k is the momentum. The gapless mode give rise to a very high electron mobility $\mu \sim 15,000\ \mathrm{cm}^2\ \mathrm{V}^{-1}\ \mathrm{s}^{-1}$ at room temperature. In fact, the graphene is the most conductive material on earth. It is also known that the bilaer graphene has gapless mode with quadratic dispersion relation $E \approx \pm|k-K|^2$, where k is the momentum. Since the band gap can be controlled by applying the electric field perpendicular to the plane, it is expected bilayer graphene may realize the new device for transistor.

The existence of Dirac points for fermions on honeycomb lattice was pointed out by Wallace [6] and the linear dispersion around the Dirac points was shown by McClure [7]. It was also shown that the discrete symmetries of the honeycomb lattice guarantee the existence of the Dirac points [8], [9], [10]and its local stability [11], [12]. Later, Semenoff [13] showed that the low energy excitations around two independent Dirac points on the fermi-surface is described by two relativistic Weyl fermions having opposite chiralities, which are also regarded as massless Dirac fermion. In lattice gauge theory, there are several formulations to describe Dirac fermion on the lattice. In the staggered fermion formulation [14], the 2^{d-2}flavor Dirac fermions emerge at low energy from a single spinless fermion hopping around the d-dimensional hypercubic lattice, in close analogy to the Semenoff's model. The staggered fermion has been studied in momentum space representation [15], in which the fermion field is divided into 2^d components corresponding to the subdomains in the total momentum space and in position space formalism [16] where the 2^d spin-flavor degrees of freedom of the Dirac fermion arise from the sites within the d-dimensional hypercubic unit cell. The advantage of the position space formulation is that one can identify the the spin flavor symmetry as a local theory. Therefore the quantum number of low energy excitations is clearly identified. As a by-product, one can also construct the exact chiral symmetry at finite lattice spacing.

In the case of honeycomb lattice in 2+1 dimension, the approach by Semenoff [13] is analogous to the momentum space formulation for staggered fermion. Therefore, It is natural to expect that position space formulation might also be possible for graphene system.

In this talk, I will show how to construct the Dirac fermion in position space on honeycomb lattice in analogy with the staggered fermion [17]. Using this formalism, I will also show that there is a hidden exact "flavor-cihral" symmetry in the tight-binding Hamiltonian for graphene system.

2. Tight-binding model

The essential properties of the graphene system can be described by the tight binding model

PoS(LATTICE2014)019

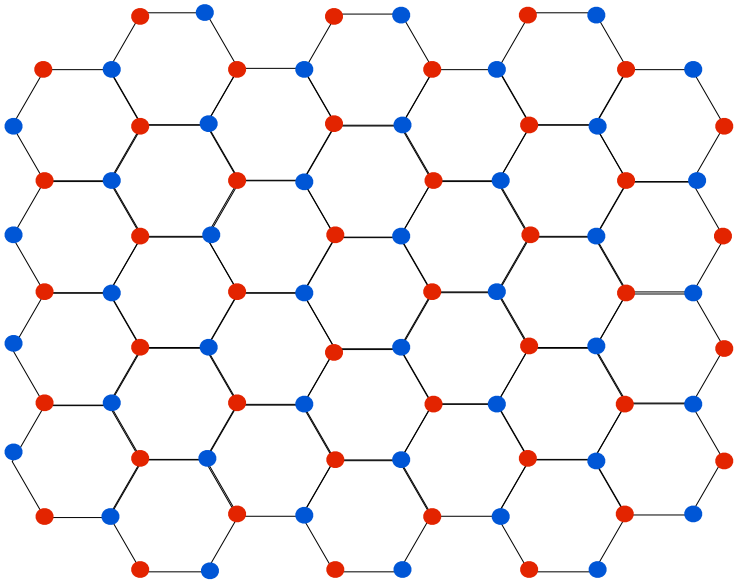

Figure 1: Honeycomb lattice is constituted of two triangular sub-lattices A and B.

on honeycomb lattice with the Hamiltonian

$$\begin{aligned}\mathscr{H} &= -t\sum_{\vec{r}\in A}\sum_{i=1,2,3}\left[a^\dagger(\vec{r})b(\vec{r}+\vec{s}_i)+b^\dagger(\vec{r}+\vec{s}_i)a(\vec{r})\right]\\ &\quad -t'\Big[\sum_{\vec{r}\in A}\sum_{j=1}^{6}a^\dagger(\vec{r})a(\vec{r}+\vec{s}'_j)+\sum_{\vec{r}\in B}\sum_{j=1}^{6}b^\dagger(\vec{r}+\vec{s}'_j)(\vec{r})\Big],\end{aligned} \tag{2.1}$$

where the first line is the nearest neighbor hopping term and the second line is the next-to-nearest neighbor hopping term, and t, t' are hopping amplitudes, whose value for the Graphene system can be estimated as $t = 2.8$ eV and $t' = 0.1$ eV [**?**]. The operators $a(a^\dagger)$ and $b(b^\dagger)$ are the fermionic annihilation (creation) operators of electrons on two triangular sublattices A and B respectively. The two dimensional vectors $\vec{s}_i (i = 1,2,3)$ and $\vec{s}'_j (j = 1,\cdots,6)$ denote the position for three nearest neighbors and the six next-to-nearest neighbors respectively. $\vec{s}_i (i = 1,2,3)$ is explicitly given as

$$\vec{s}_1 = a_0\left(1,\ 0\right),\ \ \vec{s}_2 = a_0\left(-1/2,\ \sqrt{3}/2\right),\ \ \vec{s}_3 = a_0\left(-1/2,\ -\sqrt{3}/2\right), \tag{2.2}$$

where a_0 denotes a honeycomb lattice spacing, which is estimated as $a_0 = 1.42$ Å [**?**] for the graphene. In order to find the Dirac points, we make Fourier transformation

$$a(\vec{r}) = \int\frac{d^2k}{(2\pi)^2}e^{i\vec{k}\cdot\vec{r}}\tilde{a}(\vec{k}),\ b(\vec{r}) = \int\frac{d^2k}{(2\pi)^2}e^{i\vec{k}\cdot\vec{r}}\tilde{b}(\vec{k}), \tag{2.3}$$

for the fermionic creation and annihilation operator. The nearest neighboring Hamiltonian represented in momentum space is given by

$$\mathscr{H} = \int\frac{d^2k}{(2\pi)^2}\begin{pmatrix}\tilde{a}(\vec{k})\\ \tilde{b}(\vec{k})\end{pmatrix}^\dagger\begin{pmatrix}0 & D(\vec{k})\\ D^*(\vec{k}) & 0\end{pmatrix}\begin{pmatrix}\tilde{a}(\vec{k})\\ \tilde{b}(\vec{k})\end{pmatrix} \tag{2.4}$$

PoS(LATTICE2014)019

with

$$D(\vec{k}) = t \sum_{i=1,2,3} e^{i\vec{k}\cdot\vec{s}_i}. \tag{2.5}$$

Thus the energy eigenvalue of the above Hamiltonian is represented as

$$E(\vec{k}) = \pm t \Big| \sum_{i=1,2,3} e^{i\vec{k}\cdot\vec{s}_i} \Big|. \tag{2.6}$$

In the half-filled electron system, the negative and positive eigenvalues, which corresponds to the valence band and conduction band respectively, appear, and there are two independent Dirac points $\vec{K}_\pm$, in which $E(\vec{K}_\pm) = 0$ is fulfilled, on the fermi-surface.

In order to derive the low energy effective Hamiltonian, we expand $D(\vec{k})$ around the Dirac points with respect to the momentum. Regarding $\vec{K}_\pm$ and A, B site as spin degrees of freedom (DOF), and defining four component Dirac-spinor field $\tilde{\xi}(\vec{p})$ as

$$\tilde{\xi}(\vec{p}) = \big(\tilde{a}(\vec{K}_+ + \vec{p}), \tilde{b}(\vec{K}_+ + \vec{p}), \tilde{b}(\vec{K}_- + \vec{p}), \tilde{a}(\vec{K}_- + \vec{p})\big)^T, \tag{2.7}$$

the Hamiltonian in Eq.(2.4) reads

$$\mathscr{H} \approx iv \sum_{i=1,2} \int_{\mathrm{BZ}} \frac{d^2p}{(2\pi)^2} \tilde{\xi}^\dagger(\vec{p}) \big[\hat{\gamma}_0 \hat{\gamma}_i p_i\big] \tilde{\xi}(\vec{p}). \tag{2.8}$$

Since the above is same form as the kinematic term of Dirac fermion field, $v = 3a_0t/2$ is interpreted as a fermi velocity of quasiparticles. Note that the gamma matrices $\hat{\gamma}_0, \hat{\gamma}_1, \hat{\gamma}_2$ satisfy Clifford algebra $\{\hat{\gamma}_\mu, \hat{\gamma}_\nu\} = g_{\mu\nu} \cdot 1_{4\times4}$, where $g_{\mu\nu}$ is a metric in $2+1$ dimensional space-time. Furthermore, introducing the matrix $\hat{\gamma}_3$, which is anti-commutative with $\hat{\gamma}_0, \hat{\gamma}_1, \hat{\gamma}_2$, we can define $\hat{\gamma}_5 = i\hat{\gamma}_0\hat{\gamma}_1\hat{\gamma}_2\hat{\gamma}_3$ [18], which we call as flavor-chiral symmetry forbidding a (parity-invariant) mass term $m\tilde{\xi}^\dagger\hat{\gamma}_0\tilde{\xi}$.

We notice that, in the above derivation, it is not clear whether the theory is manifestly local, because each component of fermion field is defined only in the subdomain near the low-energy points $K_\pm$ so that the continuity of the Dirac fermion in momentum space is not obvious.

3. Discrete symmetries and the Dirac points

It has been known by condensed matter physicists that the existence of the Dirac points [8], [9], [10] and their local stability [11], [12] can be understood by the discrete symmetries of the underlying lattice structure. Let us review the conventional understanding of the Dirac points.

3.1 Bloch wave function

Let us denote the wavefunctions of the valence electron around the carbon atom at A site with position $\vec{x}$ and at B site with position $\vec{x}+\vec{s}_1$ as $|A,\vec{x}\rangle$ and $|B,\vec{x}+\vec{s}_1\rangle$ respectively. One can see that the pair of lattice sites $\vec{x}$, $\vec{x}+\vec{s}_1$ form the minimal unit cell and the whole lattice has a periodicity with respect to the fundamental vectors $\vec{b}_i (i = 1,2,3)$. Although we have assigned $\vec{x}+\vec{s}_1$ for the

PoS(LATTICE2014)019

partner B, one could instead assign $\vec{x}+\vec{s}_2$ or $\vec{x}+\vec{s}_3$. The Bloch wave function with momentum $\vec{k}$ can be written as

$$|A,\vec{k}\rangle = \sum_{\vec{x}} \exp(i\vec{k}\cdot\vec{x})|A,\vec{x}\rangle,\ |B,\vec{k}\rangle = \textstyle\sum_{\vec{x}} \exp(i\vec{k}\cdot\vec{x})|B,\vec{x}+\vec{s}_1\rangle \tag{3.1}$$

Since the Hamiltonian is invariant under discrete translation $\vec{x}\to\vec{x}+\vec{b}_i (i=1,2,3)$, One can show that the Hamiltonian can be diagonalized in momentum as

$$\mathscr{H} = \int \frac{dk^2}{(2\pi)^2} (a^\dagger(k) b^\dagger(k)) \begin{pmatrix} \langle A,k|H|A,k\rangle & \langle A,k|H|B,k\rangle \\ \langle A,k|H|B,k\rangle & \langle B,k|H|B,k\rangle \end{pmatrix} \begin{pmatrix} a(k) \\ b(k) \end{pmatrix} \tag{3.2}$$

Diagonalizing the Hamiltonian, one can obtain the following dispersion relation

$$E(\vec{k}) = \frac{1}{2}\left[\langle A,k|H|A,k\rangle + \langle B,k|H|B,k\rangle \pm \sqrt{(\langle A,k|H|A,k\rangle - \langle B,k|H|B,k\rangle)^2 + 4|\langle A,k|H|B,k\rangle|^2}\right] \tag{3.3}$$

The gap vanishes only when

$$\langle A,k|H|A,k\rangle = \langle B,k|H|B,k\rangle,\ \langle A,k|H|B,k\rangle = 0. \tag{3.4}$$

holds simultaneously. In the next few subsections, we will see that the discrete symmetries of the honeycomb lattice can restrict the properties of the matrix elements in the Hamiltonian in Eq.(4.13).

3.2 Inversion symmetry

The position vectors for A site $\vec{x}_A$ and B site can be labeled by integers and vectors $\vec{s}_i (i=1,2,3)$ as

$$\begin{aligned} \vec{x}_A &= n_1\vec{s}_1 + n_2\vec{s}_2 + n_3\vec{s}_3, \\ \vec{x}_B &= \vec{s}_1 + n_1\vec{s}_1 + n_2\vec{s}_2 + n_3\vec{s}_3, \end{aligned} \tag{3.5}$$

where n_1, n_2, n_3 are arbitrary set of integers satifsfying $n_1+n_2+n_3=0$. Let us consider the inversion P with respect to the line which is perpendicular to the bond connecting the A site at the origin and the B site at $\vec{s}_1$. Under this inverstion A sites and B sites are mapped as

$$\begin{aligned} \vec{x}_A \equiv n_1\vec{s}_1 + n_2\vec{s}_2 + n_3\vec{s}_3 &\xrightarrow{P} \vec{x}'_B \equiv \vec{s}_1 + (-n_1)\vec{s}_1 + (-n_2)\vec{s}_2 + (-n_3)\vec{s}_3, \\ \vec{x}_B \equiv \vec{s}_1 + n_1\vec{s}_1 + n_2\vec{s}_2 + n_3\vec{s}_3 &\xrightarrow{P} \vec{x}'_A \equiv (-n_1)\vec{s}_1 + (-n_2)\vec{s}_2 + (-n_3)\vec{s}_3. \end{aligned} \tag{3.6}$$

Using the definition of the Bloch state and the inversion property of the honeycomb lattice, one can show after a little algebra that the Bloch wavefunctions transform under inversion as

$$P|A,\vec{k}\rangle = |B,\vec{k}_P\rangle,\quad P|B,\vec{k}\rangle = |A,\vec{k}_P\rangle, \tag{3.7}$$

where $\vec{k}_P$ is the mometum obtained from $\vec{k}$ by inversion operation P. Since the hopping probabilty respects the symmetry of the honeycomb lattice, the Hamiltonian is also invariant under inversion P. Therefore, one finds

$$\begin{aligned} \langle A,\vec{k}|H|A,\vec{k}\rangle &= \langle B,\vec{k}_P|H|B,\vec{k}_P\rangle,\quad \langle A,\vec{k}|H|B,\vec{k}\rangle = \langle B,\vec{k}_P|H|A,\vec{k}_P\rangle, \\ \langle B,\vec{k}|H|A,\vec{k}\rangle &= \langle A,\vec{k}_P|H|B,\vec{k}_P\rangle,\quad \langle B,\vec{k}|H|B,\vec{k}\rangle = \langle A,\vec{k}_P|H|A,\vec{k}_P\rangle. \end{aligned} \tag{3.8}$$

PoS(LATTICE2014)019

3.3 C_3 rotation symmetry

Let us next consider the rotation around the A site at the origin $x_A = (0,0)$. The honeycomb lattice is invariant.Under rotation by 120 degrees which we shall call 'C_3 rotation'. The C_3 rotation maps A sites and B sites as

$$\begin{aligned}\vec{x}_A \equiv n_1\vec{s}_1 + n_2\vec{s}_2 + n_3\vec{s}_3 \xrightarrow{C_3} \vec{x}'_A &\equiv n_1\vec{s}_2 + n_2\vec{s}_3 + n_3\vec{s}_1,\\ \vec{x}_B \equiv \vec{s}_1 + n_1\vec{s}_1 + n_2\vec{s}_2 + n_3\vec{s}_3 \xrightarrow{C_3} \vec{x}'_B &\equiv \vec{s}_2 + n_1\vec{s}_2 + n_2\vec{s}_3 + n_3\vec{s}_1.\\ &= \vec{s}_1 + n_1\vec{s}_2 + n_2\vec{s}_3 + n_3\vec{s}_1 + (\vec{s}_2 - \vec{s}_1).\end{aligned} \tag{3.9}$$

Note that in the above equation there appears an additional contribution $\vec{s}_2 - \vec{s}_1$ to the B site for the pair of A and B sites in a unit cell. Using the definition of the Bloch state and the inversion property of the honeycomb lattice, one can show after a little algebra

$$\begin{aligned}C_3|A,\vec{k}\rangle &= |A,\vec{k}_{C_3}\rangle\\ C_3|B,\vec{k}\rangle &= e^{i\theta(\vec{k})}|B,\vec{k}_{C_3}\rangle\end{aligned} \tag{3.10}$$

where $\vec{k}_{C_3}$ is the mometum obtained from $\vec{k}$ by inverse C_3 rotation and $\theta(\vec{k}) = \vec{k}\cdot(\vec{s}_2 - \vec{s}_1)$. Since the hopping probabilty respects the symmetry of the honeycomb lattice, the Hamiltonian is also invariant under inversion C_3. Therefore, one finds

$$\begin{aligned}\langle A,\vec{k}|H|A,\vec{k}\rangle = \langle A,\vec{k}_{C_3}|H|A,\vec{k}_{C_3}\rangle,\quad \langle A,\vec{k}|H|B,\vec{k}\rangle = e^{i\theta(\vec{k})}\langle A,\vec{k}_{C_3}|H|B,\vec{k}_{C_3}\rangle,\\ \langle B,\vec{k}|H|A,\vec{k}\rangle = e^{-i\theta(\vec{k})}\langle B,\vec{k}_{C_3}|H|B,\vec{k}_{C_3}\rangle,\quad \langle B,\vec{k}|H|B,\vec{k}\rangle = \langle B,\vec{k}_{C_3}|H|B,\vec{k}_{C_3}\rangle.\end{aligned} \tag{3.11}$$

3.4 Existence of Dirac points

If there exists a special momentum $\vec{k}^*$ which is a simultaneous fixed point under inversion P and C_3 rotation i.e. $\vec{k}^*_P = \vec{k}^*_{C_3} = \vec{k}^*$, Eqs (3.8), (3.11) give

$$\begin{aligned}\langle A,\vec{k}^*|H|A,\vec{k}^*\rangle &= \langle B,\vec{k}^*|H|B,\vec{k}^*\rangle,\\ (e^{i\theta(k^*)} - 1)\langle A,\vec{k}^*|H|B,\vec{k}^*\rangle &= 0.\end{aligned} \tag{3.12}$$

When the phase $\theta(k^*)$ is nontrivial, Eq.(3.12) implies that the Hamiltonian is proportional to identity matrix so that the two eigenvalues coincide which means that there is no gap at $\vec{k} = \vec{k}^*$. In fact, the Dirac points $\vec{K}_\pm$ are the only simultaneous fixed points under P and C_3 with nontrivial phases $\theta(\vec{K}_+), \theta(\vec{K}_-)$. Therefore, one finds that the existence of the gapless points is guaranteed by the discrete symmetries of the honeycomb lattice without depending on the details of the Hamiltonian.

3.5 Local stability of the Dirac points

It is also known that under a certain condition, the Dirac points can be stable against any small detuning of the parameters of the Hamiltonian, such as small distortions of the honeycomb lattice etc. To discuss it, let us reparameterizing the matrix elements in Eq.(2.1) as

$$\langle A,\vec{k}|H|A,\vec{k}\rangle \equiv R_0(\vec{k}) + R_3(\vec{k}),\ \langle A,\vec{k}|H|B,\vec{k}\rangle \equiv R_1(\vec{k}) - iR_2(\vec{k}),\ \langle B,\vec{k}|H|B,\vec{k}\rangle \equiv R_0(\vec{k}) - R_3(\vec{k}), \tag{3.13}$$

PoS(LATTICE2014)019

where $R_0(\vec{k}), R_i(\vec{k})(i=1,2,3)$ are real functions of $\vec{k}$. Then, the energy eigenvalue for the general Hamiltonian can be written as

$$E(\vec{k}) = R_0(\vec{k}) \pm \sqrt{(R_1(\vec{k}))^2 + (R_2(\vec{k}))^2 + (R_3(\vec{k}))^2} \tag{3.14}$$

Regarding the functions $R_i(\vec{k})(i=1,2,3)$ as the map from the two dimensional Brillouin zone (BZ) to three dimensional Euclidean space R^3,

$$\vec{k} \to \vec{R}(\vec{k}), \tag{3.15}$$

the energy gap $2\sqrt{R_1^2+R_2^2+R_3^2}$ is the minimum distance between the mapped torus in the target space and the origin. Gapless means that the torus in R^3 touches the origin. Since the detunings of the Hamiltonian correspond to the deformation of the map from the BZ to R^3, it is easy to see that one requires a fine-tuning in order for the mapped torus to remain touching the origin after deformation, which means that under arbitrary detuning the gap is unstable.

However, there is an excemption. if there is a special symmetry in the Hamiltonian, the gap can be stable. For example, when the Hamiltonian has a Z_2 symmetry

$$\{H, \sigma_3\} = 0, \tag{3.16}$$

where $\sigma_3 = \begin{pmatrix} 1 & 0 \\ 0 & -1 \end{pmatrix}$, $R_3(\vec{k}) = 0$. In this case, the functions $R_i(\vec{k})(i=1,2,3)$ always becomes a map from the two dimensional BZ to two dimensional Euclidean space R^2. If the mapped torus contains the origin in R^2, it is obvious that the mapped torus also contains the origin after any small deformation which keeps the Z_2 symmetry. The tight-binding Hamiltonian with only nearest neighbor hopping terms is such an example.

The above arguments on the properties of the Dirac points based on the discrete symmetries and the Dirac points is quite general and is independent of the details of the Hamiltonian. On the other hand, whether there exists an exact continuous flavor-chiral symmetry at finite lattice spacing is unknown. Since the exact symmetry predicts the Nambu-Goldstone mode if there occurs a spontaneous symmetry breaking, it can affect the low energy dynamics. In the next section, using the analogy with the staggered fermion, we reformulate the fermions on honeycomb lattice in position space, which will be useful to study the hidden exact symmetry.

4. Position space formulation

4.1 Staggered fermion

The staggered fermion action in two dimension, for example, is

$$S = \frac{1}{2}\sum_x \sum_{\mu=1}^{2} \bar{\chi}(x)\eta_\mu(x)(\chi(x+\hat{\mu}) - \chi(x-\hat{\mu})). \tag{4.1}$$

with $\eta_1(x) = 1$ and $\eta_2(x) = (-1)^{x_1}$. In position space formalism, one relabels the lattice sites (x_1,x_2) as $(x_1,x_2) = (2X_1+\rho_1, 2X_2+\rho_2)$ with X_1, X_2 being integers and $\rho_1, \rho_2 = 0,1$. Relabeling also the fermion fields by introducing new fermion fields $\psi_\rho(X)$ as

$$\psi_{\rho_1,\rho_2}(X_1,X_2) \equiv \chi(x_1,x_2) \tag{4.2}$$

PoS(LATTICE2014)019

This means the original lattice sites are decomposed into 1) internal degrees of freedom corresponding to the unit cell and 2) position degrees of freedom with lattice spacing which is twice as big as the original lattice spacing. In Fourier space, the original BZ is enfolded into smaller region so that all the zero points of the kinetic term of the massless staggered fermion are at the origin of the new BZ. The lattice action with relabeled fields can be written as

$$S = \sum_X \sum_{\rho,\rho'} \sum_\mu \bar{\psi}(X) \left[(\Gamma_\mu)_{\rho,\rho'} \nabla_\mu - \frac{i}{2} (\Lambda_\mu)_{\rho,\rho'} \Delta_\mu \right] \psi_{\rho'}(X). \tag{4.3}$$

Here we have matrices Γ_μ, Λ_μ are defined as

$$\Gamma_1 = \tau_1 \otimes 1, \;\; \Gamma_2 = \tau_3 \otimes \sigma_1, \;\; \Lambda_1 = \tau_2 \otimes 1, \;\; \Lambda_2 = \tau_3 \otimes \sigma_2, \tag{4.4}$$

and the difference operators ∇_μ, Δ_μ are defined as

$$\begin{aligned} \nabla_\mu \psi(X) &= \frac{1}{2} [\psi(X+\hat{\mu}) - \psi(X-\hat{\mu})], \\ \Delta_\mu \psi(X) &= \frac{1}{2} [\psi(X+\hat{\mu}) + \psi(X-\hat{\mu}) - 2\psi(X)], \end{aligned} \tag{4.5}$$

with $\hat{\mu}$ being the unit vector in μ direction. Int this formulation, one can see that the action takes the form of two flavor Dirac fermion with the naive kinetic term and the flavored-Wilson term. The flavored-Wilson term partially breaks the $SU(2)$ chiral symmetries and there remains a $U(1)$ chiral symmetry

$$\delta\psi(X) = \Gamma_5 \psi(X), \;\; \delta\bar{\psi}(X) = \bar{\psi}(X)\Gamma_5, \tag{4.6}$$

where $\Gamma_5 = \tau_3 \otimes \sigma_3$. In what follows, we study the analogous construction for fermions on honeycomb lattice.

4.2 Tight binding model on honeycomb lattice in the position space formulation

First we consider the new labeling of DOF of the fermionic creation and annihilation operator as shown in Figure 2. In this labeling, we define $A\rho$ and $B\rho$ ($\rho = 0,1,2$) as the new DOF having the operators on the site of honeycomb lattice. $\chi^\dagger_{I\rho}(\vec{x}), \chi_{I\rho}(\vec{x})$ are the new definition of creation and annihilation operators (the mass dimension of this operator is $\mathcal{O}(m)$.). The arguments $\vec{x}, \vec{y}$ are the positions of the center of hexagonal unit cell on the fundamental lattice,

$$\vec{e}_0 = a\left(1,\, 0\right), \;\; \vec{e}_1 = a\left(-1/2,\, \sqrt{3}/2\right), \;\; \vec{e}_2 = a\left(-1/2,\, -\sqrt{3}/2\right), \tag{4.7}$$

where a is the new lattice spacing defined as a distance between hexagonal unit cells. The triangular sublattice $I(=A,B)$ of honeycomb lattice is composed of hexagonal unit cells bounded by red circles in Figure 2. Note that the summation of three unit vectors vanishes as $\vec{e}_0 + \vec{e}_1 + \vec{e}_2 = 0$ [1]

[1] Here we note that there is following relation between $\vec{e}_\rho (\rho = 0,1,2)$ and $\vec{s}_i (i = 1,2,3)$:

$$\vec{e}_0 = 3\vec{s}_1, \;\; \vec{e}_1 = 3\vec{s}_2, \;\; \vec{e}_2 = 3\vec{s}_3. \tag{4.8}$$

PoS(LATTICE2014)019

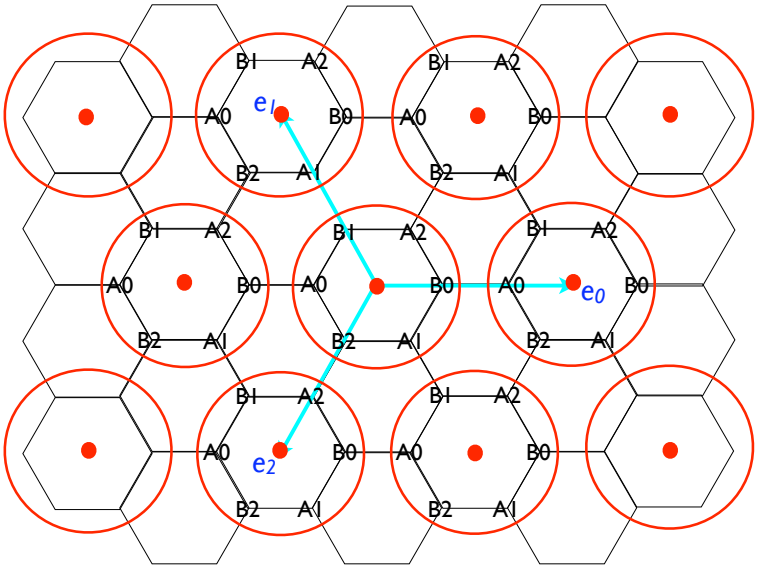

Figure 2: Honeycomb lattice

Defining the first and second derivative operators in $\vec{e}_\rho$ directions on the fundamental lattice as

$$\nabla_\rho = \frac{1}{2}(T_\rho^\dagger - T_\rho), \quad \Delta_\rho = \frac{1}{2}(T_\rho + T_\rho^\dagger - 2), \tag{4.9}$$

H can be also represented as

$$H(\vec{x},\vec{y}) = \tau_1 \otimes M\delta_{\vec{x},\vec{y}} - i\sum_\rho (\tau_2 \otimes \Gamma_\rho)\nabla_\rho(\vec{x},\vec{y}) + \frac{1}{2}\sum_\rho (\tau_1 \otimes \Gamma_\rho)\Delta_\rho(\vec{x},\vec{y}), \tag{4.10}$$

, where

$$M = \begin{pmatrix} 1 & 1 & 1 \\ 1 & 1 & 1 \\ 1 & 1 & 1 \end{pmatrix}, \ \Gamma_0 = \begin{pmatrix} 1 & 0 & 0 \\ 0 & 0 & 0 \\ 0 & 0 & 0 \end{pmatrix}, \ \Gamma_1 = \begin{pmatrix} 0 & 0 & 0 \\ 0 & 1 & 0 \\ 0 & 0 & 0 \end{pmatrix}, \ \Gamma_2 = \begin{pmatrix} 0 & 0 & 0 \\ 0 & 0 & 0 \\ 0 & 0 & 1 \end{pmatrix}. \tag{4.11}$$

Now the first and the second terms in Eq.(4.10) are interpreted as the mass term and the kinetic term in the continuum limit ($a \to 0$), and also the third term vanishes, which is the second derivative term, in the continuum limit.

In the Fourier transformed language, we have

$$\mathscr{H} = \int \frac{d^2k}{(2\pi)^2} \tilde{\psi}(\vec{k})^\dagger \tilde{H}(\vec{k}) \psi(\vec{k}), \tag{4.12}$$

where

$$\tilde{H}(\vec{k}) = \tau_1 \otimes M + \sum_\rho (\tau_2 \otimes \Gamma_\rho)\sin k_\rho + \sum_\rho (\tau_1 \otimes \Gamma_\rho)(\cos k_\rho - 1), \tag{4.13}$$

PoS(LATTICE2014)019

with $k_\rho = \vec{k}\cdot\vec{e}_\rho$. In order to give an intuitive picture for the eigenmodes of the Hamiltonian, we first consider the low energy limit, $k_\rho \to 0$, where the χ approaches to the constant field. In this limit, the Hamiltonian is

$$H^{\rm low} \equiv \lim_{\vec{k}\to 0} t\tilde{H}(\vec{k}) = t(\tau_1 \otimes M), \tag{4.14}$$

and using

$$\tilde{\chi}_{I\rho}(\vec{k}) = \frac{1}{\sqrt{3}} \sum_{\rho'=0,1,2} e^{i2\pi\rho\rho'/3} \psi_{I\rho'}(\vec{k}), \tag{4.15}$$

one easily sees the diagonalized form

$$H^{\rm low} = t(\tau_1 \otimes M^{\rm diag}), \tag{4.16}$$

with

$$M^{\rm diag} = \begin{pmatrix} 3 & 0 & 0 \\ 0 & 0 & 0 \\ 0 & 0 & 0 \end{pmatrix}. \tag{4.17}$$

This implies that the constant mode can be decomposed into two massless modes and one massive mode. Integrating out the massive mode $\tilde{\psi}_{I0}(\vec{k})$, the Hamiltonian is reduced to the following form

$$\mathscr{H}_{\rm ef} = \int_{-\pi/a}^{\pi/a} \frac{d^2k}{(2\pi)^2} \tilde{\psi}^\dagger(\vec{k}) \Big[v\Big\{ k_1(\tau_2\otimes\sigma_1) + k_2(\tau_2\otimes\sigma_2) \Big\} + \mathscr{O}(k^2) \Big] \tilde{\psi}(\vec{k}), \tag{4.18}$$

$$\tilde{\psi}(\vec{k}) = \Big(\tilde{\psi}_{A1}(\vec{k}) \;\; \tilde{\psi}_{A2}(\vec{k}) \;\; \tilde{\psi}_{B1}(\vec{k}) \;\; \tilde{\psi}_{B2}(\vec{k}) \Big)^T, \tag{4.19}$$

with $v = at/2$. In the above tensor product representations, the latter of tensor structure acts on flavor space of physical mode $a = 1,2$.

In the continuum limit, the effective Hamiltonian has the following 4 global symmetries,

$$1_{2\times2}\otimes 1_{2\times2},\;\; \tau_1\otimes\sigma_3,\;\; \tau_2\otimes 1_{2\times2},\;\; \tau_3\otimes\sigma_3. \tag{4.20}$$

Now we consider the existence of parity invariant mass term in the Hamiltonian. This term is invariant under the parity transformation (which is exchange symmetry of $A \leftrightarrow B$ and $x \to -x$ but $\rho \to \rho$ in Figure 2), and so that we have

$$m\tilde{\psi}^\dagger(\vec{k})(\tau_1\otimes 1_{2\times2})\tilde{\psi}(\vec{k}). \tag{4.21}$$

This is invariant under two global symmetries, $1_{2\times2}\otimes 1_{2\times2},\;\; \tau_1\otimes\sigma_3$, whereas, under symmetry generated by $\tau_2\otimes 1_{2\times2}$, $\tau_3\otimes\sigma_3$, this mass term is not invariant. Therefore, in analogy to QCD, we shall call the symmetry with generator $\tau_2\otimes 1_{2\times2}$, $\tau_3\otimes\sigma_3$ as "flavor-chiral symmetry". Under this global symmetry, the parity invariant mass term Eq.(4.21) is forbidden up to the first order of $\vec{k}$ (see in Table 1). We notice that the higher derivative term than $\mathscr{O}(k^2)$ violates "flavor-chiral symmetry" similar to Wilson fermion.

In the continuum limit, there exists a global flavor-chiral symmetry generated by $\tau_3\otimes\sigma_3$, however, as in the case of overlap fermion in lattice QCD, such global symmetry may be deformed by lattice artifact at finite lattice spacing. In the next section, we consider a possibility of flavor-chiral symmetry on position space formulation in honeycomb lattice.

PoS(LATTICE2014)019

Table 1: Symmetry in effective theory for parity invariant mass term.

Global symmetry			
preserved		broken	
$1_{2\times2}\otimes 1_{2\times2}$	$\tau_1\otimes\sigma_3$	$\tau_2\otimes 1_{2\times2}$	$\tau_3\otimes\sigma_3$

5. Hidden exact symmetry

Let us now discuss the exact flavor-chiral symmetry at finite lattice spacing. We look for the possibility that flavor-chirial symmetry in the continuum may be preserved by adding a modification term of $O(ak)$ where k is the momentum. Namely, the exact chiral symmetry for the Fourier transform of the fermion field $\tilde{\psi}(k)$ can be described as

$$\begin{aligned}\delta\tilde{\psi}(k) &= \Gamma_5(k)\tilde{\psi}(k),\\ \Gamma_5(k) &= \Gamma_5^{\rm cont}+O(ak)\end{aligned} \tag{5.1}$$

The condition for the exact flavor-chiral symmetry is

$$[\tilde{H}(k),\Gamma(k)]=0. \tag{5.2}$$

Expanding the Hamiltonian in Eq.(4.13) and $\Gamma_5(k)$ in powers of ak, and substituting into Eq.(5.2), we can determine the momentum expansion coefficients for $\Gamma_5(k)$ order by order. For the flavor-chiral symmetry corresponding to $\tau_2\otimes 1_{2\times2}$ in the continuum, we cannot find the solution of Eq.(5.2) at second order in ak, wheres fro the flavor-chiral symmetry corresponding to $\tau_3\otimes\sigma_3$ we can find the solution of Eq(5.2) at least through third order in ak.

Based on this experience in momentum expansion, we employ the following ansatz for exact flavor-chiral symmetry of Hamiltonian

$$\begin{aligned}\delta\chi(\vec{x}) &= i\theta\Gamma_5\chi(\vec{x})\\ &= i\theta\Big[(\tau_3\otimes X)\chi(\vec{x})+\frac{1}{2}\sum_\rho(\tau_3\otimes Y_\rho)(\Delta_\rho\chi(\vec{x})+2\chi(\vec{x}))+\frac{1}{i}\sum_\rho(1\otimes Z_\rho)(\nabla_\rho\chi(\vec{x}))\Big],\end{aligned} \tag{5.3}$$

where X,Y_ρ, and Z_ρ are unknown 3×3 Hermitian matrices. Based on this ansatz, we determine the form of X,Y_ρ, and Z_ρ from the solution of symmetry equation $[\tilde{H},\tilde{\Gamma}_5]=0$ in the momentum representation. $\tilde{\Gamma}_5$ is defined as in momentum representation, which is consistent with generator $\tau_2\otimes 1_{2\times2}$ of global flavor-chiral symmetry in the continuum limit Iimposing $[\tilde{H}(\vec{k}),\tilde{\Gamma}_5(\vec{k})]=0$, we obtain following equations;

$$\{\Lambda,X\}+\sum_\rho(\Gamma_\rho W_\rho+W_\rho^\dagger\Gamma_\rho)=0 \tag{5.4}$$

$$\{\Gamma_\rho,X\}+\Lambda W_\rho^\dagger+W_\rho\Lambda=0 \tag{5.5}$$

$$\Lambda W_\rho+W_\rho^\dagger\Lambda+\sum_{\sigma\neq\lambda\,(\sigma,\lambda\neq\rho)}(\Gamma_\sigma W_\lambda^\dagger+W_\lambda\Gamma_\sigma)=0 \tag{5.6}$$

$$\Gamma_\rho W_\rho^\dagger+W_\rho\Gamma_\rho=0 \tag{5.7}$$

$$\Gamma_\rho W_\sigma+W_\sigma^\dagger\Gamma_\rho=0\ (\rho\neq\sigma), \tag{5.8}$$

PoS(LATTICE2014)019

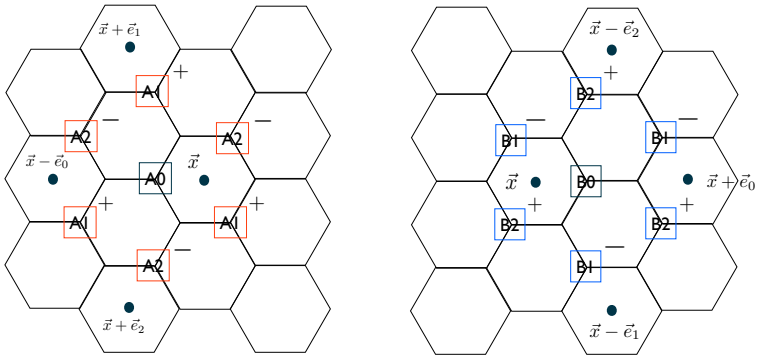

Figure 3: Geometrical picture flavor-chiral transformationof Left and right panel show transformation for $\chi_{A0}(\vec{x})$ and one for $\chi_{B0}(\vec{x})$ respectively. The transformation for $\chi_{A0}(\vec{x})$ ($\chi_{B0}(\vec{x})$) involves $\chi_{A\rho}(\vec{x})$ ($\chi_{B\rho}(\vec{x})$) surrounded by red (blue) square, where sign denotes its overall factor.

where $W_\rho \equiv \frac{1}{2}(Y_\rho + iZ_\rho)$. We obtain the explicit forms of X, Y_ρ, and Z_ρ as

$$X = \begin{pmatrix} 0 & -i & i \\ i & 0 & -i \\ -i & i & 0 \end{pmatrix}, \tag{5.9}$$

$$Y_0 = \begin{pmatrix} 0 & -i & i \\ i & 0 & 0 \\ -i & 0 & 0 \end{pmatrix}, \; Y_1 = \begin{pmatrix} 0 & -i & 0 \\ i & 0 & -i \\ 0 & i & 0 \end{pmatrix}, \; Y_2 = \begin{pmatrix} 0 & 0 & i \\ 0 & 0 & -i \\ -i & i & 0 \end{pmatrix}, \tag{5.10}$$

$$Z_0 = \begin{pmatrix} 0 & -1 & 1 \\ -1 & 0 & 0 \\ 1 & 0 & 0 \end{pmatrix}, \; Z_1 = \begin{pmatrix} 0 & 1 & 0 \\ 1 & 0 & -1 \\ 0 & -1 & 0 \end{pmatrix}, \; Z_2 = \begin{pmatrix} 0 & 0 & -1 \\ 0 & 0 & 1 \\ -1 & 1 & 0 \end{pmatrix}. \tag{5.11}$$

Next we consider how such flavor-chiral symmetry is interpreted as on honeycomb lattice. Rewriting Eq.(5.3) in components of $\chi(\vec{x})$, the transformation for $\chi_{A\rho}(\vec{x})$, $\chi_{B\rho}(\vec{x})$ reads

$$\begin{aligned} \delta\chi_{A\rho}(\vec{x}) &= \theta\big[\chi_{A_{\rho+1}}(\vec{x}+\vec{e}_{\rho+1}) - \chi_{A_{\rho-1}}(\vec{x}-\vec{e}_\rho) \\ &\quad + \chi_{A_{\rho+1}}(\vec{x}-\vec{e}_\rho) - \chi_{A_{\rho-1}}(\vec{x}+\vec{e}_{\rho-1}) + \chi_{A_{\rho+1}}(\vec{x}) - \chi_{A_{\rho-1}}(\vec{x})\big], \end{aligned} \tag{5.12}$$

$$\begin{aligned} \delta\chi_{B\rho}(\vec{x}) &= \theta\big[-\chi_{B_{\rho+1}}(\vec{x}-\vec{e}_{\rho+1}) + \chi_{B_{\rho-1}}(\vec{x}+\vec{e}_\rho) \\ &\quad - \chi_{B_{\rho+1}}(\vec{x}+\vec{e}_\rho) + \chi_{B_{\rho-1}}(\vec{x}-\vec{e}_{\rho-1}) - \chi_{B_{\rho+1}}(\vec{x}) + \chi_{B_{\rho-1}}(\vec{x})\big]. \end{aligned} \tag{5.13}$$

One can see that the flavor-chiral transformation involves the next-to-nearest neighbor sites with alternating signs as in Figure 3. Using the conventional formulation as in Eq.(2.1), the flavor-chiral transformation of $a(\vec{x})$, $b(\vec{x})$ is expressed as

$$\delta a(\vec{x}) = \theta[a(\vec{x}+\vec{s}_2-\vec{s}_3) - a(\vec{x}-\vec{s}_1+\vec{s}_2) + a(\vec{x}+\vec{s}_3-\vec{s}_1)$$

PoS(LATTICE2014)019

$$-a(\vec{x}-\vec{s}_2+\vec{s}_3)+a(\vec{x}+\vec{s}_1-\vec{s}_2)-a(\vec{x}-\vec{s}_3+\vec{s}_1)] \tag{5.14}$$

$$\delta b(\vec{x}) = \theta[b(\vec{x}+\vec{s}_2-\vec{s}_3)-b(\vec{x}-\vec{s}_1+\vec{s}_2)+b(\vec{x}+\vec{s}_3-\vec{s}_1)$$
$$-b(\vec{x}-\vec{s}_2+\vec{s}_3)+b(\vec{x}+\vec{s}_1-\vec{s}_2)-b(\vec{x}-\vec{s}_3+\vec{s}_1)] \tag{5.15}$$

If we take a continuum limit $a \to 0$, the above flavor-chiral transformation becomes $\delta\chi(\vec{x}) = \theta[X + \sum_\rho Y_\rho]\chi(\vec{x}) = 3i\theta X\chi(\vec{x})$. In the mass basis, X is transformed to the following form,

$$\begin{pmatrix} 0 & 0 & 0 \\ 0 & 1 & 0 \\ 0 & 0 & -1 \end{pmatrix}, \tag{5.16}$$

except for an overall factor. Thus, the exact flavor-chiral symmetry corresponds to the global flavor-chiral symmetry $\tau_3 \otimes \sigma_3$ as expected. The flavor-chiral symmetry in the low energy effective theory has been discussed in some literature (see a review [18]).

In the bilayer graphene, one has A sites and B sites in the upper layer and $\tilde{A}$ sites and $\tilde{B}$ sites in the lower layer. In the AB stacked bilayer graphene, the B sites in the upper layer sit on top on $\tilde{A}$ sites in the lower layer. In this system, there appears an additional inter-layer hopping term in the Hamiltonian

$$H_{\text{inter}} = \int \frac{d^2k}{(2\pi)^2}(a^\dagger(k)b^\dagger(k)) \begin{pmatrix} 0 & 0 \\ \gamma & 0 \end{pmatrix} \begin{pmatrix} \tilde{a}(k) \\ \tilde{b}(k) \end{pmatrix} \tag{5.17}$$

It is interesting to see that the flavor-chiral symmetry

$$\phi = i\theta\Gamma_5\psi,\ \tilde{\phi} = i\tilde{\theta}\Gamma_5\tilde{\psi} \tag{5.18}$$

is preserved even with the interlayer hopping term, where ψ and $\tilde{\psi}$ are fermions in the upper and lower layers provided that we set $\theta = \tilde{\theta}$ [19].

6. Summary

We discussed the low energy behavior of the fermions on honeycomb lattice. Conventially the existence of the Dirac points and the local stability against small detuning can be understood by the discrete symmetries of the honeycomb lattice.

We gave an alternative interpretation why there exists a massless Dirac fermion using the analogy with the staggered fermion. Reformulating the fermions on honeycomb lattice in position space, we interpret that the (pseudo-)spin and flavor degrees of freedom arise from the unit hexagonal lattice. We also find that the hidden exact symmetry corresponding to the partial U(1) flavor-chiral symmetry at finite lattice spacing. This symmetry guarantees this existence of the massless Dirac fermion at low energy. The position space formulation easily extends toward the gauge interacting system. This also has the complementary information for understanding of the connection with honeycomb lattice simulation [20, 21] Monte-Carlo simulation with electron-electron interaction [22, 23] and QED simulation with 2+1 dimensional fermion [25, 26].

PoS(LATTICE2014)019

Acknowledgments

I woud like to thank my collaborator Masaki Hirotsu, Eigo Shintani and Aya Kagimura. This work is supported by the Grant-in-Aid of the Japanese Ministry of Education (No. 26400248).

References

[1] K. S. Novoselov, A. K. Geim, S. V. Morozov, D. Jiang, Y. Zhang, S. V. Dubonos, I. V. Grigorieva, and A. A. Firsov, Science **306**, 666 (2004)

[2] K. S. Novoselov, A. K. Geim, S. V. Morozov, D. Jiang, M. I. Katsnelson, I. V. Grigorieva, S. V. Dubonos and A. A. Firsov, Nature **438**, 197 (2005) [cond-mat/0509330 [cond-mat.mes-hall]].

[3] Y. Zhang, Y. -W. Tan, H. L. Stormer and P. Kim, Nature **438**, 201 (2005).

[4] M. I. Katsnelson, K. S. Novoselov, and A. K. Geim, Nature Physics 2, 620 (2006), arXiv:cond-mat/0604323

[5] D. C. Elias, R. V. Gorbachev, A. S. Mayorov, S. V. Morozov, A. A. Zhukov, P. Blake, L. A. Ponomarenko, I. V. Grigorieva, K. S. Novoselov, F. Guinea and A. K. Geim, Nature Physics **8**, 172 (2012).

[6] P. R. Wallace: Phys. Rev. 71, 622 (1947).

[7] J. W. McClure: Phys. Rev. 104, 666 (1956)

[8] W. M. Lomer: Proc. Roy. Soc.(London), A227, 330 (1955).

[9] J. C. Slonczewski and P. R. Weiss: Phys. Rev. 109, 272 (1958)

[10] T. Morimoto and M. Koshino: Phys. Rev. B 87, 085424 (2013).

[11] C. Herring: Phys. Rev. 52, 365 (1937).

[12] K. Asano and C. Hotta: Phys. Rev. B 83, 245125 (2011).

[13] G. W. Semenoff, Phys. Rev. Lett. **53**, 2449 (1984).

[14] L. Susskind, Phys. Rev. D **16**, 3031 (1977).

[15] H. S. Sharatchandra, H. J. Thun and P. Weisz, Nucl. Phys. B **192**, 205 (1981);
C. van den Doel and J. Smit, Nucl. Phys. B **228**, 122 (1983);
M. F. L. Golterman and J. Smit, Nucl. Phys. B **245**, 61 (1984).

[16] H. Kluberg-Stern, A. Morel, O. Napoly and B. Petersson, Nucl. Phys. B **220**, 447 (1983).

[17] M. Hirotsu, T. Onogi and E. Shintani, Nucl. Phys. B **885**, 61 (2014) [arXiv:1303.2886 [hep-lat]].

[18] V. P. Gusynin, S. G. Sharapov and J. P. Carbotte, Int. J. Mod. Phys. B **21**, 4611 (2007) [arXiv:0706.3016 [cond-mat.mes-hall]].

[19] M. Hirotsu, A. Kagimura, T. Onogi, E. Shintani, in progress.

[20] R. Brower, C. Rebbi and D. Schaich, PoS LATTICE **2011**, 056 (2011) [arXiv:1204.5424 [hep-lat]].

[21] P. V. Buividovich and M. I. Polikarpov, Phys. Rev. B **86**, 245117 (2012) [arXiv:1206.0619 [cond-mat.str-el]].

[22] J. E. Drut and T. A. Lähde, Phys. Rev. Lett. **102**, 026802 (2009); J. E. Drut and T. A. Lähde, Phys. Rev. B **79**, 165425 (2009).

PoS(LATTICE2014)019

[23] W. Armour, S. Hands, C. Strouthos, Phys. Rev. B **81**, 125105 (2010).

[24] P. V. Buividovich, E. V. Luschevskaya, O. V. Pavlovsky, M. I. Polikarpov and M. V. Ulybyshev, Phys. Rev. B **86**, 045107 (2012) [arXiv:1204.0921 [cond-mat.str-el]].

[25] E. V. Gorbar, V. P. Gusynin and V. A. Miransky, Phys. Rev. D **64**, 105028 (2001) [hep-ph/0105059].

[26] E. Shintani and T. Onogi, arXiv:1203.1091 [hep-lat]; E. Shintani and T. Onogi, PoS LATTICE **2012**, 062 (2012) [arXiv:1211.6495 [hep-lat]].

PoS(LATTICE2014)019